Short-Term Prediction of Deflection for a Steel Truss Railway Bridge Induced by Train Load using Seasonal ARIMA: A Case Study at BH 77 Bridge, Lampung, Indonesia

Fauzi Dwi Setiawan[1], Emeralda Insani Nuansa[1,*], Hanafi Isnanta Prabawa[1], Thiya Fiantika[1], M. Rosyidi[2], Farhan Muzzammil Ali[1]

[1]Research Centre for Transportation Technology, National Research and Innovation Agency of Indonesia, South Tangerang, 15314, Indonesia
[2]Marine Bioindustry Laboratory, National Research and Innovation Agency of Indonesia, North Lombok, 83352, Indonesia

*Author to whom correspondence should be addressed:
E-mail: emer001@brin.go.id

(Received May 28, 2025; Revised September 02, 2025; Accepted December 16, 2025)

Abstract: The BH 77 Railway Bridge is one of the railway bridges that withstands the heaviest train load in Indonesia. The Babaranjang train, which crosses this track in South Sumatra, consists of 60 wagons and 2 locomotives, all loaded with coal. This heavy load is considered extreme, especially since the bridge was designed in the 1970s under an older structural design code. Therefore, a structural health monitoring system (SHMS) is essential to prevent a bridge's sudden failure. One of the key advances in Structural Health Monitoring System is predicting structural responses based on historical measurement data. This study focuses on developing a deflection prediction model using seasonal ARIMA. The bridge deflection is a critical parameter in structural health monitoring; thus, two pressure transducer sensors were installed at the end of the bridge near the abutment and reservoirs as a water level references were placed on the midspan of the bridge to measure the actual deflection induced by the train load. Eight days deflection data was analyzed, focusing on the trains loaded with coal (the heaviest train), and assuming a consistent average speed for all trains. The seasonal ARIMA was then performed to analyze the optimal frequency model. Utilizing Mean Absolute Error (MAE) and Root Mean Square Error (RMSE) evaluation techniques, this model is appropriate for short-term deflection prediction models, with results showing an MAE range from 13% to 16% and RMSE 16%-21%. The outcomes of this model's development are particularly promising and provide a general overview of the trainload-induced bridge deflection prediction.

Keywords: ARIMA; Deflection Prediction; Railway Bridge; Structural Health Monitoring

1. Introduction

Structural failure monitoring has become a concern among engineers as sudden failures increasingly occur. Particularly on the bridge structures, which are essential in connecting areas separated by rivers and/or ravines and assuring the safety of transportation while passing through the bridge. Bridges experience deterioration and potential collapse due to complex factors such as environmental load variations, natural disasters, and material degradation[1,2)]. As the actual load applied shows a significant increase, and the design code used was the former code, many bridge structures need to be monitored continuously. The former load according to RM 1921, only considered the internal load applied on the bridge, such as the dead load and moving load of the train. However, the latest code was revised into a code published by the Ministry of Transportation of the Republic of Indonesia titled Railway Track Technical Requirement by adding external loads, such as wind load, impact load, horizontal load, seismic load, temperature load, etc[3)].

Some indicators can be used to evaluate structural health conditions: natural frequency, deflection, and strain[4)]. The most practical and significant evaluation metric for assessing the general condition of bridges is deflection[5)]. As the most apparent indicator of bridge deformation, deflection can be utilized for evaluating a bridge's quality,

Cite: F. Setiawan et al., "Short-Term Prediction of Deflection for a Steel Truss Railway Bridge Induced by Train Load using Seasonal ARIMA: A Case Study at BH 77 Bridge, Lampung, Indonesia". Evergreen, 12 (04) 2112-2124 (2025). https://doi.org/10.5109/7402641.

operational circumstances, and stiffness[6]. Moreover, deflections are considered to be one of the most accurate indicators of overall structural behaviour[7]. Multiple standards underscore the necessity of monitoring and managing vertical displacement in railway bridges, proposing for the assessment of permissible vertical deflection at mid-span. These include the Design Guide for Steel Railway Bridges of the UK (2004), UIC CODE 518 OR (2009), and the Guideline of Track Maintenance of the Korea Rail Network Authority (2016)[6,8–10].

Multiple types of sensor systems are employed to monitor bridge deflection. The two most common types of measurement systems are indirect measurement systems and vision-based systems. Often used as an indirect measure method, inclinometers are utilized to measure bridge deflection[11,12]. Inclinometers establish a theoretical reference displacement trajectory, illustrating the deflection experienced by a finite element model when a unit load is applied at various structural positions[6]. The structural monitoring systems that are GPS-based can also be used to monitor the condition of structures, and they are primarily utilized on long-span bridges or taller buildings because of their poor measurement accuracy and expensive maintenance[13–15]. A vision-based monitoring system using a drone to capture structural response under seismic excitation was explored by Luna et. al, showing a wider range of vision-based tools[16]. Among the vision-based dynamic deflection measuring systems that may produce long-term remote and automated bridge deflection measurements are laser scanning, photogrammetric methods, and laser Doppler instruments[3,5,17]. The results of earlier research showed that vision-based monitoring systems required a sophisticated approach for accurately determining the true displacement and were susceptible to the effects of rainy or foggy weather.

While deflection monitoring technology for railway bridges has advanced recently, researchers have also tested a novel method based on the hydrostatic pressure principle and a pressure transmitter. Liu et al. developed the connected pipe system (CPS) for deflection monitoring[18]. The fundamental operating principle of a pressure transmitter is the hydraulic transmission of pressure through liquid-filled pipes, which establish a connection between a fixed reference point and the measurement stations. These pipes' liquid contents fluctuate in direct proportion to the respective locations of the measurement and reference stations. Zhou et al. conducted a study that assessed the deflections of a PSC box-girder bridge utilizing an interconnected pipe system for health monitoring and condition assessment. A deflection-based multilevel assessment method was introduced, wherein bridge condition is evaluated by separating deflection components attributed to traffic loading, temperature variation, and long-term effects[19]. Another study presented by Z.-K. Lee et al. utilized a fiber Bragg grating (FBG) to monitor vertical displacements of a damaged bridge structure, which also incorporates differential settlement measurement. This system operates based on the hydrostatic liquid leveling principle, which involves connected buoyancy, vessels, force equilibrium, and the photoelastic effect of FBGs[20].

In addition, advanced structural monitoring techniques play an important role in predicting and assessing the performance of bridges. The prediction of the structural responses would help in determining maintenance actions to prevent severe failure of the structure[21]. An improved variational mode decomposition (IVMD), auto-regression integrated moving average (ARIMA), and conditional kernel density estimation (CKDE) prediction of bridge deformation was put out by Xin et al.[21]. Using the empirical mode decomposition and Hilbert transform, this technique avoids disturbing insignificant components while optimizing decomposition level numbers. This approach is more effective at collecting deformation data and generating more accurate and reliable predictions of outcomes. For forecasting bridge structure deformation, Xin et al. proposed integrating the generalized autoregressive conditional heteroskedasticity (GARCH), Kalman filter, and ARIMA[22]. The five-step prediction's mean absolute error can be improved by 10.12% with this strategy. Bian et al. proposed a CEEMDAN-ARIMA model in a separate study to forecast strain sensor data for bridge monitoring. The model uses the CEEMDAN approach to first decompose the monitoring data, and then ARIMA is used to forecast the result[23].

Despite advancements in SHM, few studies comprehensively evaluate ARIMA-based forecasting models for steel truss railway bridges under extreme loads, with limited suitability assessments of ARIMA for short-term deflection predictions using real-world data. This study aims to address this research gap by employing an ARIMA-based predictive model to monitor and forecast deflection trends in the BH 77 railway bridge, Indonesia, using actual sensor-acquired deflection data. In the context of SHMS, predicting the deflection of the bridge structure will reflect the variation in train loads during specific monitoring periods. This, in turn, will help determine the maintenance strategy when there are indications that there is severe damage to the structure. This work contributes to the field by validating the accuracy of ARIMA models in SHM applications and offering information about the feasibility of real-time predictive monitoring for railway bridges.

2. Methodology

The BH 77 Bridge, as shown in Figure 1, is a railway bridge located in Tegineneng, Kab. Lampung Selatan, Provinsi Lampung, Indonesia. This bridge is a single-track steel truss railway bridge with a length of 61.6 m, a height

of 8 m, and a width of 4.8 m.

This research aims to analyze the predicted deflection for the steel truss railway bridge. The prediction would assist in forecasting future structural responses by monitoring the deflection of the railway bridge, thereby aiding in the development of a maintenance plan. The deflection data were collected through a sensor system consisting of a closed pipe system of deflection meters. With the advancement of IoT technology, the system can accommodate a real-time data transfer[24]. IoT enables smart devices to communicate and adapt dynamically, supported by low-latency edge processing that improves data throughput and responsiveness[25]. The data is then collected through a logger and transferred to the server, where it is processed using the seasonal ARIMA model to predict the deflection.

2.1. Data Acquisition

In this study, bridge monitoring used a pressure transmitter to measure the bridge's deflection. A pressure transmitter is a device used for remote monitoring and control that measures hydraulic pressure and converts it into an electrical signal. The pressure transmitter sensor uses a system called the connected pipe system (CPS). Figure 2 shows the concept of CPS.

During the bridge monitoring, pressure is generated through a combined system consisting of a water tank, a water level sensor, and a connecting pipe. The water tank is strategically positioned at a designated height associated with the design specifications. The water pipe is put longitudinally along the bridge beam, and pressure transmitters are installed at the monitored position. When train loads are applied, the pipe attached to the bridge flexes, while the water tank liquid level remains constant, causing a change in the pipe's pressure.

The schematic process of CPS for bridge deflection monitoring is illustrated in Figure 3. P1 represents the reference point's pressure, and when the pressure at time 0 is measured, it can be defined by equation 1.

$$P_{1,0} = \rho g H_{1,0} \quad (1)$$

where ρ is the water's density, g is the gravitational acceleration, and $H_{1,0}$ is the height distinction between P_1 and the liquid surface. For P_i , the pressure level at the i-th (i = 1,2,3,…,n) measurement point is defined as:

$$P_{i,0} = \rho g H_{i,0} \quad (2)$$

where $H_{i,0}$ denotes the level gap between i-th measurement point and the liquid surface. Therefore, the deviation in height between the i- th measurement point the reference point and (P_i and P_1) is

$$\Delta H_{i,0} = H_{i,0} - H_{1,0} = \frac{P_{i,0} - P_{i,0}}{\rho g} \quad (3)$$

The time when the train load passes over the bridge is denoted as T. Consequently, the pressure and measurement values at the i-th measurement point and the reference point vary over time, leading to changes in the height difference between these points.

(a)

(b)

Fig. 1: (a) side view of BH 77; (b) front view of BH 77

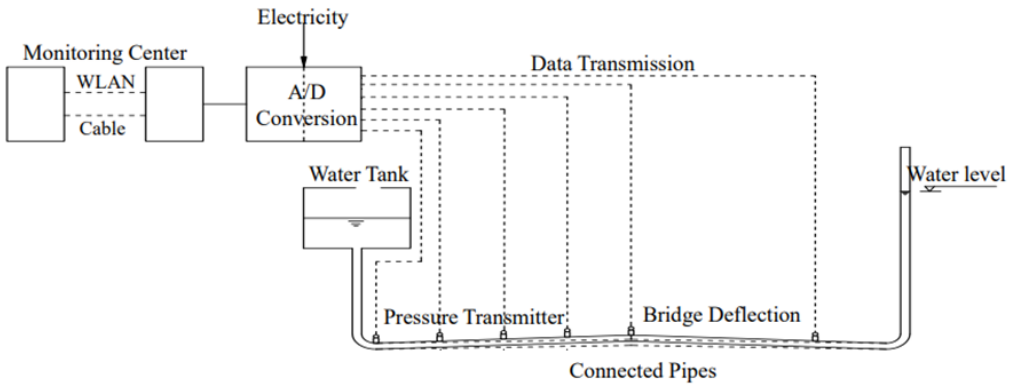

Fig. 2: The principles of CPS for bridge monitoring[5]

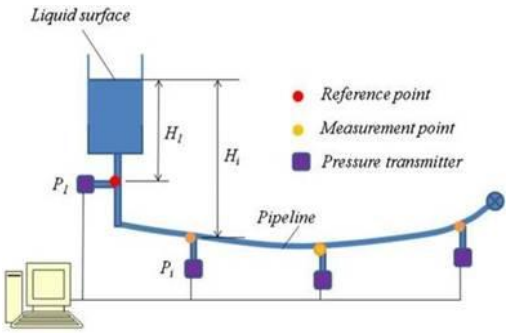

Fig. 3: CPS Schematic Diagram for Monitoring Bridge Deflection[6)]

$$\Delta H_{i,T} = H_{i,T} - H_{1,T} = \frac{P_{i,T} - P_{i,T}}{\rho g} = \frac{\Delta P_{1,T}}{\rho g} \quad (4)$$

The i-th deflection measurement point corresponding to the initial value is written as

$$D_{i,T} = \Delta H_{i,T} - \Delta H_{i,0} = \frac{\Delta P_{1,T} - \Delta P_{i,0}}{\rho g} \quad (5)$$

This study used several instruments to monitor bridge structures. The sensors placed in the BH 77 railway bridge are subsidence sensors, strain gauges, accelerometers, and passive infrared sensors (PIR). A subsidence sensor measures bridge deflection using a hydraulic method, where a pressure transmitter detects changes in liquid levels. This system operates based on the principle of pressure variation, allowing accurate monitoring of structural subsidence and deformation. It consists of three main parts: pipes that connect the reference point and pressure transmitter, water that fills the pipes, and a pressure transmitter that measures changes in liquid height. The strain gauge sensors measure strain within the truss bridge. Additionally, accelerometers are used to measure acceleration and vibrations within the structure, providing valuable data for assessing dynamic behavior[26)]. A remote sensing method using a passive sensor system was used in this study[27)]. This sensor helps detect moving objects towards the bridge and is called a passive infrared sensor (PIR), which triggers the data logger to start recording sensor data. Figure 4 and Figure 5 provide a detailed overview of the instruments used in this study.

The instrument installation is divided into two areas: outside and inside the bridge area. The determination of sensor placement is based on the critical points identified through structural analysis using finite element analysis. The instruments that were installed in the outside area of the bridge are the data logger, passive infrared sensor (PIR), and solar panels, whereas the instruments that were installed inside the bridge area are the Modbus, subsidence sensors, accelerometer, strain gauge, box panel, and solar panels that provide energy for the Modbus system. The subsidence sensor consists of a pressure transmitter and reservoir. The pressure transmitter sensors were placed at

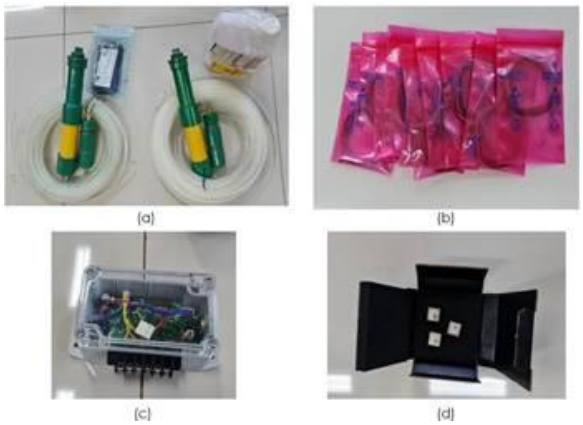

Fig. 4: (a) pressure transducer sensor; (b) strain gauges; (c) modbus controller; (d) accelerometer

Fig. 5: (a) subsidence sensor; (b) PIR sensor; (c) modbus controller; (d) data logger; (e) strain gauge sensor

the bridge end, and the reservoirs were located parallel in the middle of the bridge, while strain gauges were located at the critical points. Ideally, the pressure transmitter sensor should be placed in the middle of the bridge so it can directly respond to changes caused by the train. However, in practice, the vibrations generated by the train are too strong, preventing the pressure transmitter sensor from accurately reading the data. After conducting repeated tests in the laboratory, our team decided to change the position of the pressure transmitter sensor to the reservoir. This decision was based on the test results, which showed no difference in readings when the position was changed. The detailed installation of each instrument is shown in Figure 6.

2.2. Data Selection

This study collected data from the BH 77 railway bridge, a regular crossing point for Babaranjang trains. As shown in Figure 7, Babaranjang trains are the heaviest and most frequent trains passing over this bridge. Each train set

consists of 60 coal wagons and two CC 205 (EMD GT38ACe) locomotives, transporting coal from Tanjung Enim, Palembang, to Tarahan, Lampung. The Babaranjang train has a maximum load capacity of 50 tons per wagon and operates at a maximum speed of up to 80 km/h. At this speed, it takes between 60 and 90 seconds to cross the bridge; thus, the data captured during that duration will be used for the deflection prediction of the BH 77 bridge.

Based on Figure 8 above, eight days of deflection data recorded between 3rd February 2023 and 10th February 2023, consisting of approximately 10,000 data points induced by the Babaranjang trains was collected. Due to the challenges encountered during on-site data collecting, additional data sampling was difficult to obtain. In this study, we exclusively concentrate on the deflection data from the pressure transmitter sensor, as it provides full-day data. In contrast, complete full-day data obtained from the accelerometer and strain gauge sensors were unavailable due to data transmission errors. Hence, the eight-days deflection data collected from the pressure transmitter sensor was immediately analyzed, and short-term deflection prediction was performed.

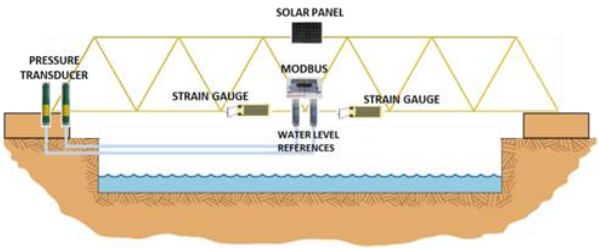

Fig. 6: Schematic diagram of sensor placement

Fig. 7: Babaranjang Train

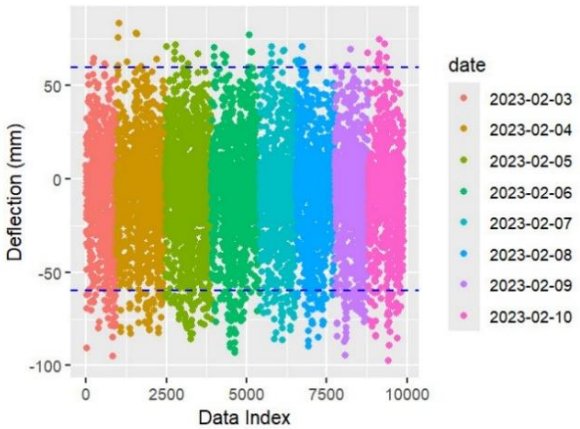

Fig. 8: Deflection Data of BH 77 Bridge induced by Babaranjang Train crossing over the bridge

2.3. Data Analysis

The raw deflection data were filtered using Kalman Filter method to reduce noise in measurements and help estimate the real-time state of the structure. The Kalman Filter (KF) provides the best estimates of the state by minimizing the mean-square error[28]. Then, a global forecast for eight days of deflection data was analyzed using Seasonal ARIMA to obtain the overall prediction. Subsequently, a daily forecast was conducted to assess the reliability of the SARIMA model. It is crucial to acknowledge that, although the train departure schedule is set by the railway company, it is often not strictly followed and is instead influenced by the daily coal transport demand. As a result, the total number of Babaranjang trains passing through the bridge may vary each day. The model was then evaluated using MAE and RSME metrics.

The maximum allowable deflection for serviceability limit state (SLS), according to the regulation of the Minister of Transportation No. 60 of 2012 on technical requirements for railway tracks, is L/1000 for the entire frame under locomotive loads, where L represents the bridge span. Therefore, the maximum permissible deflection for the BH 77 railway bridge, with a length of 61.6 m, is 61.6 mm. This value represents the safety limit for the bridge frame with respect to deflection under the serviceability llimit state (SLS). A probabilistic analysis was subsequently conducted to calculate the likelihood of the deflection exceeding the threshold. This analysis helps assess the safety index (β) of the railway bridge structure, which can be expressed in Equation 6[29].

$$\beta = Z = \Phi^{-1}(P(\delta > \delta_{threshold}) \quad (6)$$

Where Φ^{-1} represents the inverse cumulative distribution function (CDF) of the standard normal distribution and ($P(\delta > \delta_{threshold})$ denotes the probability of the deflection exceeding the threshold. Based on the Eurocode EN 1990, the probability of failure, Pf, can be expressed using a performance function, g, where a structure is deemed to survive if $g > 0$ and to have failed if $g < 0$. The performance function is defined as $g = R - E$, where R represents the resistance and E represents the response to actions. Under the serviceability limit state (SLS), R represents the deflection limit of L/1000, while E corresponds to the measured deflection. The calculated reliability index was assessed in accordance with the Eurocode standard EN 1990:2002, which specifies target reliability indices for structures of various reliability classes. Then a finite element model was developed to analyze potential failure

at the midspan based on the measured maximum deflection as a reference.

2.4. SARIMA Method

ARIMA (AutoRegressive Integrated Moving Average) models serve as the foundation for SARIMA (Seasonal AutoRegressive Integrated Moving Average). ARIMA integrates autoregressive, moving average, and differencing components. However, when dealing with seasonal patterns of time series data at fixed intervals, the standard ARIMA model may fall short. In such cases, SARIMA, or Seasonal ARIMA, becomes a more suitable option[30]. SARIMA effectively manages intricate recurring patterns and seasonal changes, typical in financial and construction data[31]. With its flexibility and capability to detect complex patterns and dynamic data, this model proves invaluable for decision-making and future predictions.

SARIMA incorporates seasonal fluctuations in time series data and is an ARIMA (Autoregressive Integrated Moving Average) extension model[32,33]. A common approach to writing the SARIMA model is as SARIMA (p, d, q) (P, D, Q), with p, d, and q stand for the autoregression order, degree of trend difference, and order of moving average, respectively, while P, D, and Q refer to the seasonal component.

The SARIMA framework modeling procedure is divided into three stages: series stability, model identification and estimation, and model diagnostics.

● **Series Stability**: This stage involves converting the time series data into a more stationary format, often through differencing. Differences are expressed as I(d), where "d" is the trend difference degree. The I(d) formula is presented in equation 7.

$$\nabla^d Yt=(1-B)^d Yt \qquad (7)$$

● **Model Identification and Estimation:** During this stage, the parameters of the ARIMA and SARIMA models are determined according to the analysis of the autocorrelation function (ACF) and partial autocorrelation function (PACF), along with iterative experimentation and testing. Autoregressive (AR) Component Formula:

$$Yt=c+\phi 1Yt-1+\phi 2Yt-2+\ldots+\phi pYt-p+\varepsilon t \qquad (8)$$

Yt in equation 8 denotes the value at time t, ϕ indicates the lagged terms coefficient (weights), Y_{t-1} … Y_{t-2} represents previous time steps (lags), and ε_t specifies the error term or noise at time t (also known as white noise). Moving Average (MA) Component Formula:

$$Yt=c+\varepsilon t+\theta 1\varepsilon t-1+\theta 2\varepsilon t-2+\ldots+\theta q\varepsilon t-q \qquad (9)$$

Based on equation 9 above, Yt denotes the value at time t, μ represents the time series average, ε_{t-1} … ε_{t-2} denotes the error term from previous time steps, θ_1 represents the coefficients for the moving average terms, and ε_t denotes the current error term.

● **Model Diagnostic**: After estimating the SARIMA model, it's crucial to examine its residuals to ensure that no patterns remain in the model residuals. This involves residual analysis, such as the ACF (Autocorrelation Function) of residuals, and tests for heteroskedasticity.

2.5. Evaluation Method

The performance of the SARIMA model was evaluated using statistical metrics of MAE (Mean Absolute Error) and RMSE (Root Mean Squared Error)[34]. MAE calculates the mean magnitude of difference between actual values and predicted values. MAE is one of the simplest methods to measure the error in a model's prediction. Equation (10) shows the formulae of MAE.

$$MAE = \frac{1}{n}\sum_{i=1}^{n}|y_i - \hat{y}_i| \qquad (10)$$

Where n is number of data points, y_i is actual value, and $\hat{y}_i$ is predicted value.

The steps to calculate MAE are as follows :

Calculate the absolute difference. It computes the discrepancy between the obseved value y_i and the predict value $\hat{y}_i$.

Take the absolute value. This serves to ensure the errors, whether positive or negative, are still counted as positive numbers that represent the magnitude of the difference, not the direction.

Calculate the mean of all the absolute error values to determine the MAE.

RMSE calculates the square root of the mean squared differences between actual and predicted values. The formulae is shown in equation (11)

$$RMSE = \sqrt{\frac{1}{n}\sum_{i=1}^{n}(y_i - \hat{y}_i)^2} \qquad (11)$$

The working principle of RMSE is as follows:

Calculate the error. Find the difference between each actual value y_i and its predicted value $\hat{y}_i$.

Square each error. This removes negative signs and gives more weight to larger errors.

Average the squared errors: Compute the Mean Squared Error (MSE).

Take the square root of the MSE: This returns the error to the original unit of measurement, resulting in the Root Mean Squared Error (RMSE).

Cite: F. Setiawan et al., "Short-Term Prediction of Deflection for a Steel Truss Railway Bridge Induced by Train Load using Seasonal ARIMA: A Case Study at BH 77 Bridge, Lampung, Indonesia". Evergreen, 12 (04) 2112-2124 (2025). https://doi.org/10.5109/7402641.

3. Results and Discussion

3.1. SARIMA Analysis Result

The SARIMA analysis began by comparing several candidate parameter configurations using AIC (Akaike Information Criterion) and BIC (Bayesian Information Criterion) to reconcile model fit with its complexity, thereby avoiding overfitting. To increase computational efficiency, different parameter combinations were explored systematically instead of using the whole auto ARIMA selection method, which might be time-consuming and computationally costly for big datasets and various parameter candidates. After exploring several candidate parameters, the best ARIMA model identified, with the lowest AIC and BIC values, corresponds to a seasonal value of 60. Lower AIC and BIC values indicate a less complex model and fits the data well with fewer parameters. Figure 9 illustrates the best AIC and BIC with a seasonal value of 60. The optimal SARIMA model with the obtained parameters: p=5, d=0, q=1, P=1, D=1, Q=0, and S=60.

The seasonal value of 60 was used because it corresponds to the duration of Babaranjang train passing over the bridge, which takes about 60 seconds with a 1 Hz sampling rate. This value reflects the actual train passing duration and represents the deflection cycle generated by a single train passing, establishing a clear physical basis for the seasonal component.

After obtaining the best SARIMA model, the global prediction for eight days of deflection data was obtained. The results show that the model can capture the deflection trends, as shown in Figure 10. The RMSE and MAE obtained respectively 31.12 mm and 24.14 mm, suggest that the error magnitudes are considerably high in comparison to the data range of about 181 mm (minimum: -97.63 mm, maximum: 83.32 mm). The high RMSE and MAE indicate that the model may encounter difficulties with extreme fluctuations, either due to measurement noise, environmental influences, or unaccounted variances.

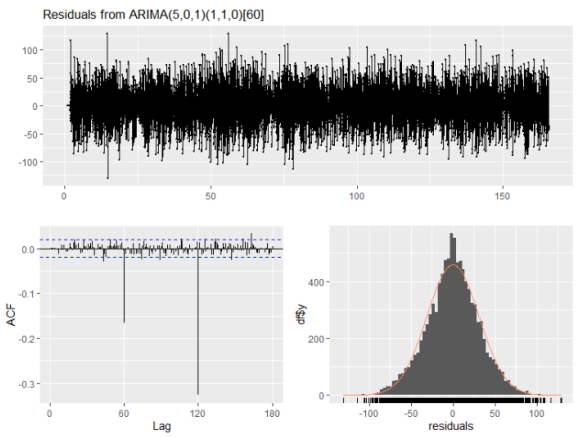

Fig. 9: Residual plot, corresponding ACF plot, and histogram from ARIMA model (5,0,1)(1,1,0)[60]

Enhancing the model parameters or integrating supplementary data sources could enhance its forecast accuracy for extreme events.

A daily forecast scenario was performed and evaluated to assess the prediction performance. The scenario uses one day's data to predict the next day's data, with the actual results serving as validation. The seasonal ARIMA model parameters utilized for daily predictions are presented in Table 1. Figures 11, 12, 13, 14, 15, 16, 17 and 18 display the daily deflection graphs, representing the filtered data from day one to day eight. The dashed blue line represents

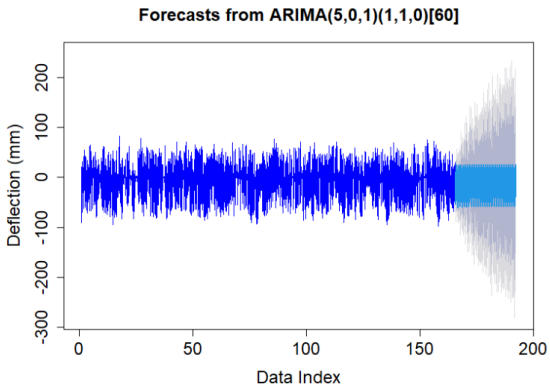

Fig. 10: Global forecast of ARIMA (5,0,1)(1,1,0)[60] using eight days deflection data

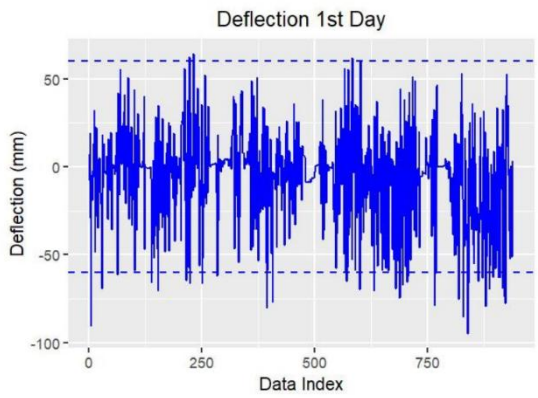

Fig. 11: Deflection graph of 1st day

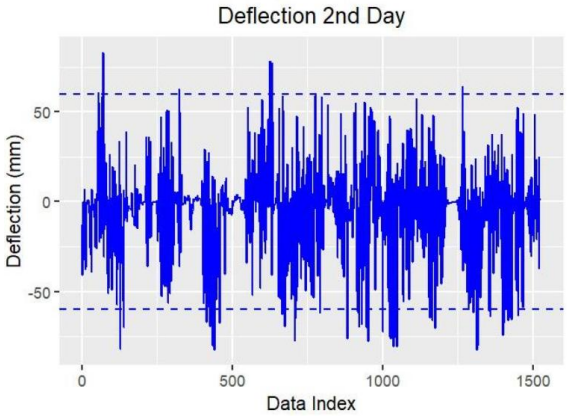

Fig. 12: Deflection graph of 2nd day

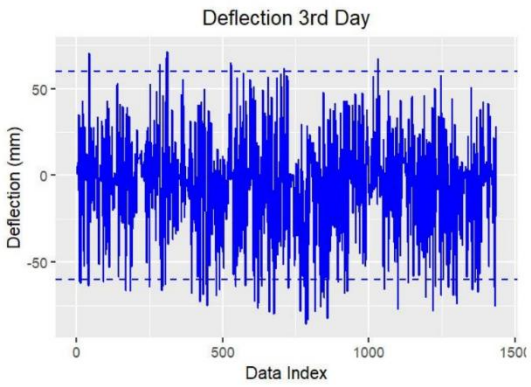

Fig. 13: Deflection graph of 3rd day

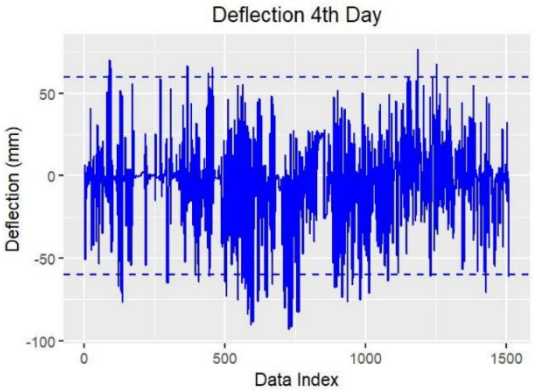

Fig. 14: Deflection graph of 4th day

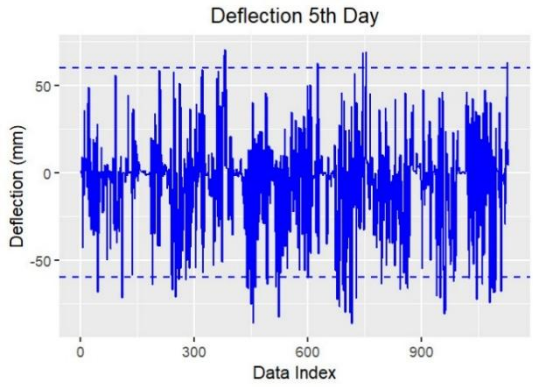

Fig. 15: Deflection graph of 5th day

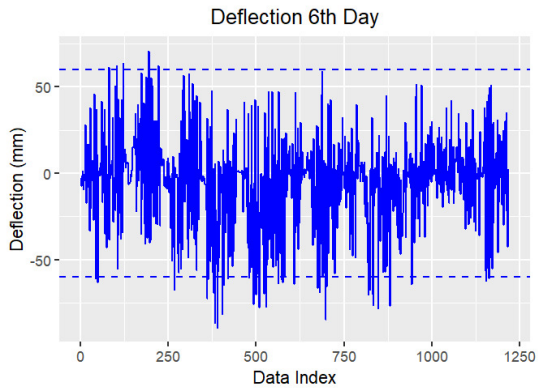

Fig. 16: Deflection graph of 6th day

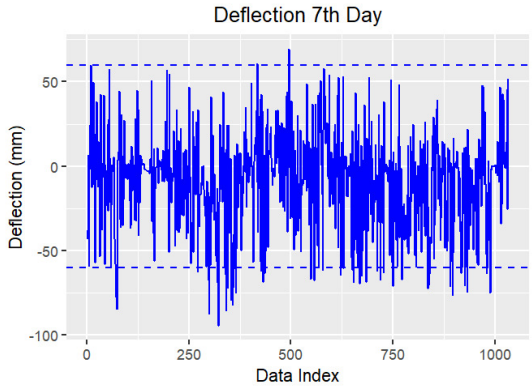

Fig. 17: Deflection graph of 7th day

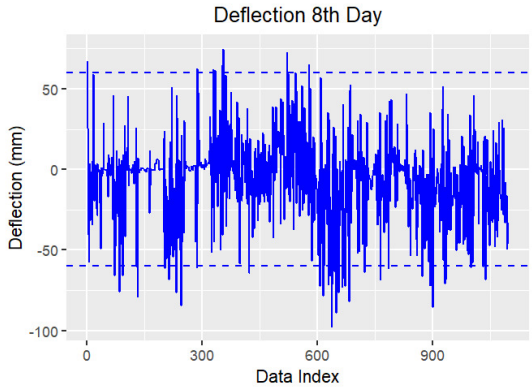

Fig. 18: Deflection graph of 8th day

the deflection threshold value of 61.60 mm. As seen, some data points exceed this threshold. Figures 19 to 25 illustrate the comparison between the predicted deflection values and the observed measurements for days two to eight, with predictions made using data from the previous day. The blue graph represents the actual deflection of the predicted day, while the red graph represents the predicted deflection based on the previous day's data. The abscissa axis represents the index of the predicted data, corresponding to the sequential time step of deflection measurement. While the y-axis represents the deflection in mm. Since the data is recorded while the train crosses the bridge, each index unit reflects a specific moment within this period, ensuring a time-aligned representation of the prediction series. The ordinate axis is the deflection value. Figure 19 shows the deflection prediction of the second day using the actual data of the first day.

This study used an optimal ARIMA configuration (p=5, d=0, q=1, P=1, D=1, Q=0, S=60), achieved MAE values between 23.02 and 30.48 and RMSE values from 30.48 to 37.7, as reported in Table 2. The data values span from –97.67 mm to 83.32 mm, providing a total range of 180.99 mm. The MAE values represent 15% to 18% of the data range, indicating that the result within an acceptable range. A lower MAE percentage indicates greater forecast accuracy. MAE below 50% can be considered "reasonable," while a value under 20% is considered

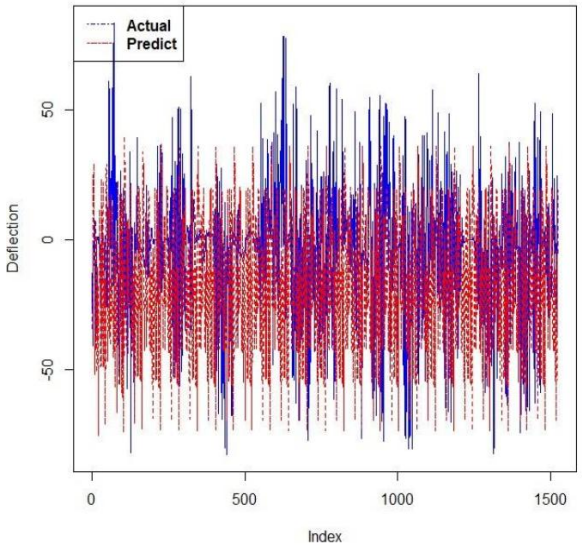

Fig. 19: Second-Day Prediction Using First-Day Data

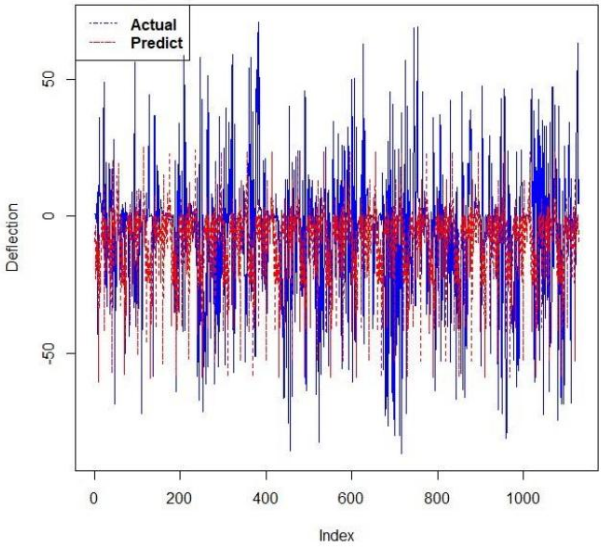

Fig. 22: Fifth-Day Prediction Using Fourth-Day Data

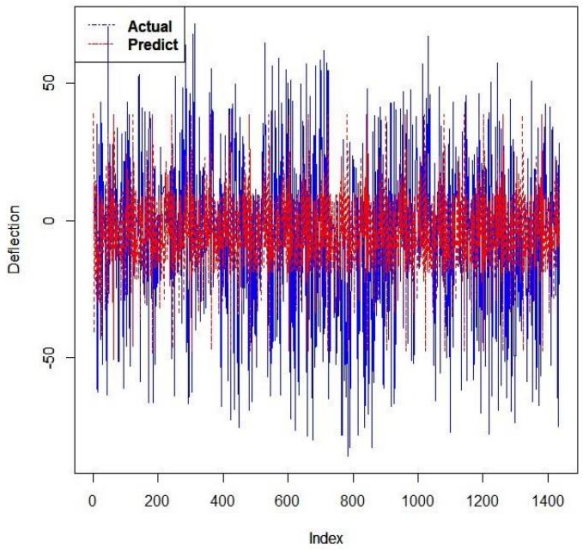

Fig. 20: Third-Day Prediction Using Second-Day Data

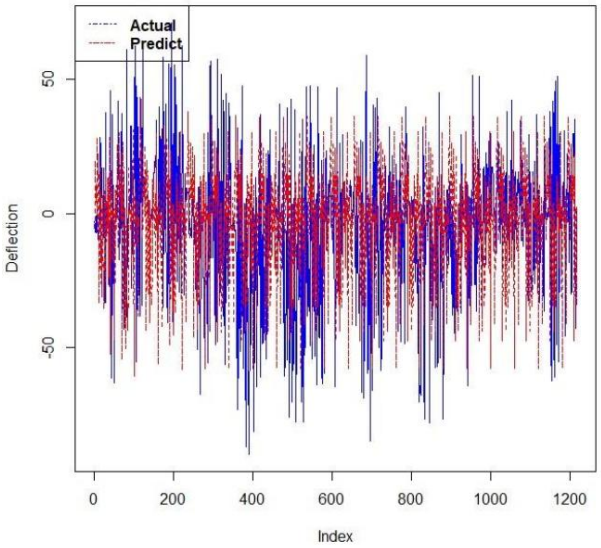

Fig. 23: Sixth-Day Prediction Using Fifth-Day Data

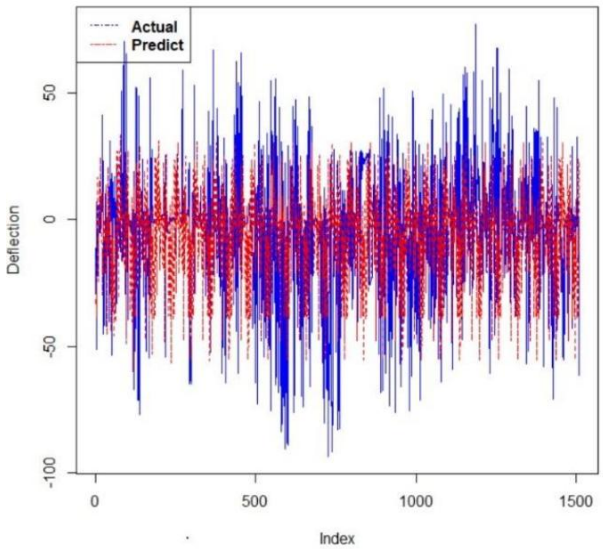

Fig. 21: Fourth-Day Prediction Using Third-Day Data

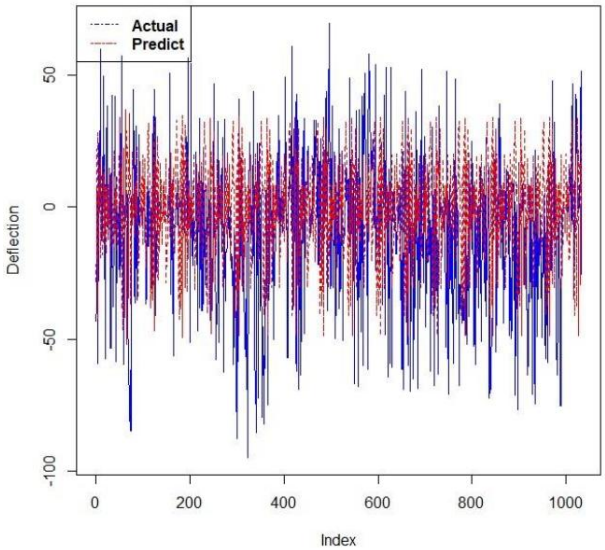

Fig. 24: Seventh-Day Prediction Using Sixth-Day Data

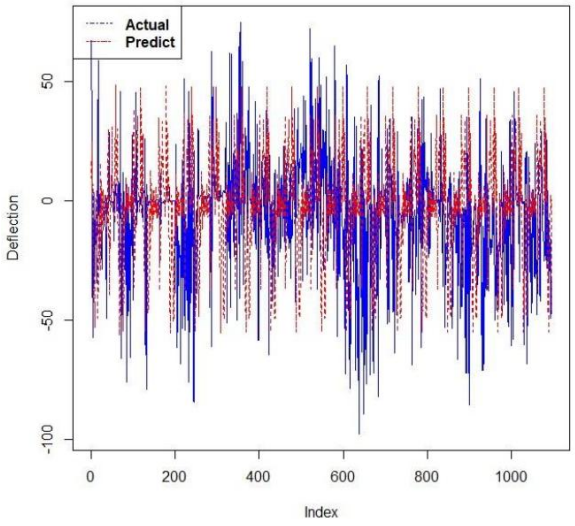

Fig. 25: Eighth-Day Prediction Using Seventh-Day Data

Similarly, the RMSE values represent that the error rate is relatively moderates with promising for future improvement. These results align with previous ARIMA-based forecasting research for structural health monitoring. Xin et al.[36] proposed an IVMD-ARIMA model that reduced mean absolute error (MAE) by 10.12% compared to conventional models.

The best prediction result was obtained in the third-day prediction using the second-day data, demonstrating the reliability of the model. The possible explanation of this result is most likely caused by the train load variation on those days is relatively similar, which leads to a good prediction result. In contrast, the worst prediction result occurred in the second-day forecast using the first-day's data. This may be due to the significant difference in train load variations between those days. Although there is a fixed schedule for train operations, it is sometimes influenced by the coal transport demand, which can cause deviation. This aspect requires further examination to determine its impact on deflection forecast accuracy, as fluctuating load distributions could significantly influence model performance.

Table 1: Sarima model parameter

Model Prediction	AIC	BIC	Order (p,d,q)	Seasonal (P,D,Q)	Frequency
day 2	8588.81	8627.04	5, 0, 1	1, 1, 0	60
day 3	14077.69	14120.01	5, 0, 1	1, 1, 0	60
day 4	13647.33	13689.14	5, 0, 1	1, 1, 0	60
day 5	14088.74	14130.86	5, 0, 1	1, 1, 0	60
day 6	10455.84	10495.64	5, 0, 1	1, 1, 0	60
day 7	11177.07	11217.5	5, 0, 1	1, 1, 0	60
day 8	9502.58	9531.86	3, 0, 1	1, 1, 0	60

The consistent performance across multiple days suggests that SARIMA effectively captures the temporal patterns in bridge deflection. However, slight variations in error values indicate potential influences from external factors such as environmental conditions and train load distribution, which should be explored further. The prediction accuracy highlights SARIMA's capability for short-term forecasting, but integrating additional features or hybrid approaches may further improve precision and robustness for real-world applications. The average error values remain within an acceptable range, indicating the practical applicability of short-term deflection forecasting. In the future, more bridges should be equipped with sensors to monitor structural health conditions, especially aging bridges. Additionally, the method needs further refinement to enable real-time monitoring of bridge conditions as well as improve the accuracy of prediction results. This suggests that while SARIMA is a viable tool for short-term bridge deflection forecasting, its performance may be enhanced through hybrid approaches, such as integrating machine learning techniques or decomposition-based pre-processing. Future studies should investigate these alternatives to further enhance the predictive capabilities of SHM systems.

Table 2: Model evaluation

Model Prediction	MAE	RMSE
day 2	30.48	37.78
day 3	25.04	31.68
day 4	25.80	33.22
day 5	23.02	30.48
day 6	24.21	31.41
day 7	26.94	34.27
day 8	25.45	32.94

3.2. Bridge Safety Evaluation

The objective of structural health monitoring is to evaluate the state and overall integrity of a bridge structure. Therefore, a probabilistic analysis of the deflection data was conducted, and the bridge's reliability was assessed in accordance with the EN 1990:2002 standard. Table 3 shows the maximum deflection for each day and the probability of the data exceeding the threshold.

Table 3: Maximum deflection per day and probability of deflection exceeding threshold

Data Day	δ_{max} (mm)	$\delta_{threshold}$ (mm)	P ($\delta > \delta_{threshold}$)
1	95.041	61.6	0.043
2	83.324	61.6	0.034
3	85.823	61.6	0.043
4	93.281	61.6	0.041
5	86.448	61.6	0.042
6	89.533	61.6	0.032
7	94.644	61.6	0.047
8	97.634	61.6	0.039

In general, deflection data exceeds the allowable threshold on a daily basis. The probability of exceedance is approximately 5%. This result can be correlated with the safety index or reliability index of the bridge structure using the First Order Reliability Method (FORM) to assess its safety level. Based on Equation 6, the reliability index is calculated using the Z-score from the normal distribution table. If we take the probability of failure, $P_f = 0.05$, then the cumulative probability is $1-0.05 = 0.95$, and the corresponding Z-score from the table is 1.645. According to EN 1990:2002, Eurocode for the basis of structural design, the reliability index target for RC3 structures is 5.3 and 4.3 for a 1-year reference period and a 50-years reference period, respectively[30]. Those reliability index values correspond to the target probability of failure which is generally very low, typically around 10^{-5} to 10^{-6} per year, depending on the risk associated with the structure. RC3 structures are associated with high-consequence class (CC3), where failure could result in very severe impacts on human life, the economy, society, or the environment. A bridge is a critical structure and is therefore classified as a CC3 (high-consequence).

The calculated daily reliability index of approximately 1.645 is significantly lower than the target value specified in EN 1990:2002. Hence, according to standard reliability criteria, the bridge is considered unsafe. Furthermore, the maximum recorded deflection of 97.6 mm exceeds the allowable limit by approximately 60%, indicating a significant serviceability violation that could result in abnormal structural behavior, potential local failures and the risk of exceeding the bridge's load-carrying capacity. Even with a low exceedance frequency of 5%, any occurrence of deflection surpassing the ultimate or serviceability limits can threaten the bridge's structural integrity.

The maximum recorded deflection was simulated using a finite element model, as shown in Figure 26. The results indicate that applying a deflection of 97.6 mm at the midspan causes one of the midspan crossbeams to enter a plastic state with the plastic equivalent strain (PEEQ) of 10.56 mm. Even at the allowable deflection limit of 61.6 mm, the crossbeam has begun to exhibit plastic behavior with the PEEQ value of 3.37 mm, as shown in Figure 27. Further analysis of the ultimate limit state with respect to material strength should be conducted in future studies.

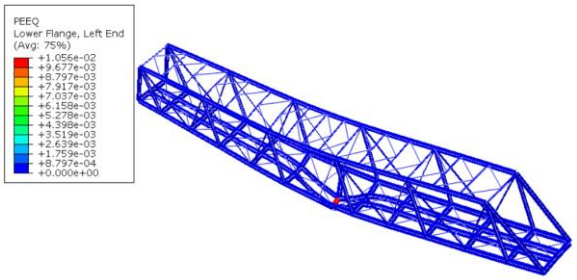

Fig. 26: Plastic Equivalent Strain in the Bridge Structure under a Midspan Deflection of 97.6 mm

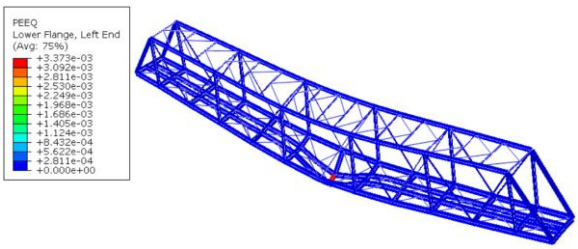

Fig. 27: Plastic Equivalent Strain in the Bridge Structure under a Midspan Deflection of 61.6 mm

4. Conclusion

This research has demonstrated that SARIMA has promising results for predicting bridge deflection data while retaining or maximizing existing raw data. The best results were obtained from analyzing deflection data using SARIMA with a frequency of 60, p = 5, d = 0, q = 1, P = 1, D = 1, Q = 0. The daily prediction results show that the MAE is in the range of 13%-16% and RMSE 16%-21%. The daily predictions yielded promising results; however, some predictions showed less accurate outcomes, possibly due to external factors such as the frequency of train loads passing over the bridge and other environmental influences. Therefore, further exploration is needed. More data sampling is required to obtain a better SARIMA model and improve prediction results.

Daily measurements indicate that the bridge deflections consistently exceed the allowable limits under the serviceability limit state (SLS). Reliability analysis yields a daily reliability index of 1.645, corresponding to a 5% probability of failure, which is substantially below the target values specified in EN 1990:2002. An exceedance of approximately 60% reflects significant serviceability violations, potentially compromising structural performance. Finite element simulations further reveal that the maximum deflection of 97.6 mm induces plastic behavior in the midspan crossbeam. These findings classify the bridge as unsafe, meaning it requires continuous monitoring and prompt maintenance. The

implementation of additional structural health monitoring devices, such as strain gauges, accelerometers, and weigh-in-motion sensors, strategically positioned along the bridge, is recommended to enhance safety assessment and early detection of critical conditions.

The connected pipe system used to measure deflection was effective in recording the data. However, due to its high sensitivity to vibration, a significant amount of noise was also recorded, requiring careful data filtering. Additionally, continuous monitoring with the CPS proved challenging, as the water inside the pipe evaporated due to the high environmental temperatures around the bridge area. As a result, the system sometimes needed to be refilled with water. In the future, it may be necessary to consider using alternative sensor systems to measure deflection on the bridge such as LVDT sensor.

Future research should include an investigation into the possibility that less accurate prediction results are caused by variations in train load over the week, as the train departure schedule is not strictly followed, not only the load from Babaranjang train, but also environmental influences such as weather and climate can affect steel structures behavior. As weather and climate change, steel structures experience temperature fluctuations, where the object is sensitive to temperature changes, both in terms of deflection and stress. Thermal sensors can be included to measure the temperature in steel structures, allowing for a deeper understanding of the relationship between temperature and steel structure behavior in the future. Additionally, integrating additional data sources from other sensors can be analyzed through multivariate forecasting models such as VARIMAX in the future research.

Acknowledgements

This research is fully supported by the National Research and Innovation Agency of Indonesia (BRIN). The authors fully acknowledged PT. Kereta Api Indonesia for the permission to data acquisition in the BH 77 railway bridge, which makes this important research viable and effective.

References

1) J.M. Ko, and Y.Q. Ni, “Technology developments in structural health monitoring of large-scale bridges,” Eng. Struct., 27 (12 SPEC. ISS.) 1715–1725 (2005). doi:10.1016/j.engstruct.2005.02.021.
2) J. Ou, and H. Li, “Structural health monitoring in mainland china: review and future trends,” Struct. Health Monit., 9 (3) 219–231 (2010). doi:10.1177/1475921710365269.
3) “Persyaratan teknis jalur kereta api,” (2011).
4) C.-C. Comisu, N. Taranu, G. Boaca, and M.-C. Scutaru, “Structural health monitoring system of bridges,” Procedia Eng., 199 2054–2059 (2017). doi:10.1016/j.proeng.2017.09.472.
5) P. Zeng, and R. Wang, “Long-term bridge deflection monitoring using a connected pipe system considering structural vibration,” IOP Conf. Ser. Earth Environ. Sci., 189 (2) 0–6 (2018). doi:10.1088/1755-1315/189/2/022007.
6) X. Ye, and B. Chen, “Condition assessment of bridge structures based on a liquid level sensing system: theory, verification and application,” Arab. J. Sci. Eng., 44 (5) 4405–4424 (2019). doi:10.1007/s13369-018-3425-6.
7) B. Torres, P. Poveda, S. Ivorra, and L. Estevan, “Long-term static and dynamic monitoring to failure scenarios assessment in steel truss railway bridges: a case study,” Eng. Fail. Anal., 152 107435 (2023). doi:10.1016/j.engfailanal.2023.107435.
8) International Union of Railways (UIC), “UIC code 518: testing and approval of railway vehicle from the point of view of their dynamic behavior-safety-track fatigue-running behavior,” (2009).
9) The Steel Construction Institute, “Design guide for steel railway bridges,” 1–136 (2004).
10) Korea Rail Network Authority, “Guideline of track maintenance,” (2016).
11) K.Y. Wong, “Instrumentation and health monitoring of cable-supported bridges,” Struct. Control Health Monit., 11 (2) 91–124 (2004). doi:10.1002/stc.33.
12) X. Hou, X. Yang, and Q. Huang, “Using inclinometers to measure bridge deflection,” J. Bridge Eng., 10 (5) 564–569 (2005). doi:10.1061/(asce)1084-0702(2005)10:5(564).
13) X. He, X. Yang, and L. Zhao, “New method for high-speed railway bridge dynamic deflection measurement,” J. Bridge Eng., 19 (7) 1–11 (2014). doi:10.1061/(asce)be.1943-5592.0000612.
14) T.-H. Yi, H.-N. Li, and M. Gu, “Recent research and applications of gps-based monitoring technology for high-rise structures,” Struct. Control Health Monit., (2012) (2012). doi:10.1002/stc.1501.
15) A. Nickitopoulou, K. Protopsalti, and S. Stiros, “Monitoring dynamic and quasi-static deformations of large flexible engineering structures with gps: accuracy, limitations and promises,” Eng. Struct., 28 (10) 1471–1482 (2006). doi:10.1016/j.engstruct.2006.02.001.
16) L. Ngeljaratan, Mohamed A. Moustafa, A. Sumarno, Agus Mudo Prasetyo, Dany Perwita Sari, and Maidina, “Exploratory study of drone data stabilization with implications in vibration-based structural health monitoring,” Evergreen, 10 (3) 1776–1783 (2023). doi:10.5109/7151727.
17) O. Ogundipe, G.W. Roberts, and C.J. Brown, “GPS monitoring of a steel box girder viaduct,” Struct. Infrastruct. Eng., 10 (1) 25–40 (2014). doi:10.1080/15732479.2012.692387.

18) Y. Liu, Y. Deng, and C.S. Cai, "Deflection monitoring and assessment for a suspension bridge using a connected pipe system: a case study in china," Struct. Control Health Monit., 22 (12) 1408–1425 (2015). doi:10.1002/stc.1751.
19) J. Zhou, Z. Sun, B. Wei, L. Zhang, and P. Zeng, "Deflection-based multilevel structural condition assessment of long-span prestressed concrete girder bridges using a connected pipe system," Measurement, 169 108352 (2021). doi:10.1016/j.measurement.2020.108352.
20) Z.-K. Lee, M. Bonopera, C.-C. Hsu, B.-H. Lee, and F.-Y. Yeh, "Long-term deflection monitoring of a box girder bridge with an optical-fiber, liquid-level system," Structures, 44 904–919 (2022). doi:10.1016/j.istruc.2022.08.048.
21) H. Ha, L.V. Manh, D.D. Nguyen, M. Amiri, I. Prakash, and B.T. Pham, "Hybrid machine learning model for prediction of vertical deflection of composite bridges," Proc. Inst. Civ. Eng. - Bridge Eng., 178 (2) 99–108 (2025). doi:10.1680/jbren.23.00007.
22) J. Xin, J. Zhou, S.X. Yang, X. Li, and Y. Wang, "Bridge structure deformation prediction based on gnss data using kalman-arima-garch model," Sens. Switz., 18 (1) (2018). doi:10.3390/s18010298.
23) S. Bian, J. Zhuo, and L. Zhu, "Strain prediction of bridge shm based on ceemdan-arima model," IOP Conf. Ser. Earth Environ. Sci., 558 (3) (2020). doi:10.1088/1755-1315/558/3/032036.
24) D. Singh, and A. Singh, "Role of building automation technology in creating a smart and sustainable built environment," Evergreen, 10 (1) 412–420 (2023). doi:10.5109/6781101.
25) A. Sharma, S. Sharma, and D. Gupta, "Ant colony optimization based routing strategies for internet of things," Evergreen, 10 (2) 998–1009 (2023). doi:10.5109/6793654.
26) T. Fiantika, W.A.N. Aspar, D.A. Purnomo, W. Barasa, S.M. Harjono, and S.P. Primadiyanti, "A review of structural health monitoring systems and application for railway bridges," AIP Conf. Proc., 2646 (2023). doi:10.1063/5.0115843.
27) A. Yussupov and Raya Z. Suleimenova, "Use of remote sensing data for environmental monitoring of desertification," Evergreen, 10 (1) 300–307 (2023). doi:10.5109/6781080.
28) K. Erazo, D. Sen, S. Nagarajaiah, and L. Sun, "Vibration-based structural health monitoring under changing environmental conditions using kalman filtering," Mech. Syst. Signal Process., 117 1–15 (2019). doi:10.1016/j.ymssp.2018.07.041.
29) "Reliability of aged offshore structures," in: Cond. Assess. Aged Struct., Elsevier, 2008: pp. 287–351. doi:10.1533/9781845695217.4.287.
30) "EN 1990:2002 eurocode for basis structural design," (2002).
31) S. Kumari, and P. Muthulakshmi, "SARIMA model: an efficient machine learning technique for weather forecasting," Procedia Comput. Sci., 235 656–670 (2024). doi:10.1016/j.procs.2024.04.064.
32) D.H.M. Aquino, "Evaluating the impacts of earthquake disasters on the building construction sector: a sarima-based counterfactual analysis," (2025).
33) D. Zhao, H. Zhang, Q. Cao, Z. Wang, and R. Zhang, "The research of sarima model for prediction of hepatitis b in mainland china," Med. U. S., 101 (23) E29317–E29317 (2022). doi:10.1097/MD.0000000000029317.
34) S. Ma, Q. Liu, and Y. Zhang, "A prediction method of fire frequency: based on the optimization of sarima model," PLoS ONE, 16 (8 August) 1–13 (2021). doi:10.1371/journal.pone.0255857.
35) H. Halidah, N. Hesty, P. Aji, Ifanda, D. Amelia, and K. Akhmad, "Short-term wind forecasting with weather data using deep learning - case study in baron techno park," Evergreen, 10 (3) 1753–1761 (2023). doi:10.5109/7151724.
36) M. Naloufi, F.S. Lucas, S. Souihi, P. Servais, A. Janne, and T. Wanderley Matos De Abreu, "Evaluating the performance of machine learning approaches to predict the microbial quality of surface waters and to optimize the sampling effort," Water, 13 (18) 2457 (2021). doi:10.3390/w13182457.
37) J. Xin, Y. Jiang, J. Zhou, L. Peng, S. Liu, and Q. Tang, "Bridge deformation prediction based on shm data using improved vmd and conditional kde," Eng. Struct., 261 (June 2021) 114285–114285 (2022). doi:10.1016/j.engstruct.2022.114285.